FM dyes enter via a store-operated calcium channel and modify calcium signaling of cultured astrocytes

Dongdong Li (李栋栋), Karine Hérault, Martin Oheim[1], and Nicole Ropert[1]

Institut National de la Santé et de la Recherche Médicale, INSERM U603, Centre National de la Recherche Scientifique, UMR 8154, Laboratoire de Neurophysiologie & Nouvelles Microscopies, Université Paris Descartes, 45 Rue des Saints Pères, F-75006 Paris, France

Edited by Thomas C. Südhof, Stanford University School of Medicine, Palo Alto, CA, and approved October 22, 2009 (received for review August 12, 2009)

The amphiphilic fluorescent styryl pyridinium dyes FM1-43 and FM4-64 are used to probe activity-dependent synaptic vesicle cycling in neurons. Cultured astrocytes can internalize FM1-43 and FM4-64 inside vesicles but their uptake is insensitive to the elevation of cytosolic calcium (Ca^{2+}) concentration and the underlying mechanism remains unclear. Here we used total internal reflection fluorescence microscopy and pharmacological tools to study the mechanisms of FM4-64 uptake into cultured astrocytes from mouse neocortex. Our data show that: (*i*) endocytosis is not a major route for FM4-64 uptake into astrocytes; (*ii*) FM4-64 enters astrocytes through an aqueous pore and strongly affects Ca^{2+} homeostasis; (*iii*) partitioning of FM4-64 into the outer leaflet of the plasma membrane results in a facilitation of store-operated Ca^{2+} entry (SOCE) channel gating; (*iv*) FM4-64 permeates and competes with Ca^{2+} for entry through a SOCE channel; (*v*) intracellular FM4-64 mobilizes Ca^{2+} from the endoplasmic reticulum stores, conveying a positive feedback to activate SOCE and to sustain dye uptake into astrocytes. Our study demonstrates that FM dyes are not markers of cycling vesicles in astrocytes and calls for a careful interpretation of FM fluorescence.

calcium homeostasis | endoplasmic reticulum | lipid bilayer | styryl dye | TIRF

In astrocytes the strong expression of the plasma membrane (PM) store-operated Ca^{2+} entry (SOCE) (1–4) contrasts with a relatively small expression of voltage-gated channels and AMPA/NMDA ligand-gated channels that are mostly expressed by neurons. In response to neuronal activity and neurotransmitter release, the activation of astroglial metabotropic receptors induces a reduction of the endoplasmic reticulum (ER) Ca^{2+} concentration ($[Ca^{2+}]_{ER}$) that leads to the activation of the SOCE and to an elevation of the intracellular Ca^{2+} concentration ($[Ca^{2+}]_i$) (4) that is critical for the electrically silent astrocytes to release gliotransmitters and control nearby neurons, glia, and blood vessels (5). The type 1–2 stromal interaction molecules (STIM1–2) and Orai1–3 membrane proteins are key components of the SOCE, being the ER Ca^{2+} sensor and the PM pore-forming subunit, respectively (6, 7). A possible participation of the classical transient receptor potential (TRPC) channels to the protein complex generating the SOCE is debated in several cell types (8), including astrocytes (3).

Styryl pyridinium FM dyes are amphiphilic molecules that reversibly partition in lipid membranes. Their positively charged pyridinium head prevents them from diffusing through the PM. Only weakly fluorescent in aqueous solution their quantum yield increases in a lipid environment. Their activity-dependent uptake and destaining has made them common probes for synaptic vesicle cycling at the nerve terminals (9–11). Cultured astrocytes internalize FM dyes (3, 12–18). However, this uptake is not modified by the activation of metabotropic glutamate receptors (19), and its mechanism remains elusive.

Here, we show that incubating astrocytes with FM4-64 for 2 to 5 min leads to an FM4-64 uptake by permeation through a channel involved in SOCE. We also show that: (*i*) insertion of FM4-64 in PM facilitates SOCE; (*ii*) like other small FM dyes (FM1-43 and FM5-95, but not FM3-25), FM4-64 permeates through a cationic aqueous pore, and acts as a permeant SOCE blocker competing with Ca^{2+} influx; (*iii*) FM4-64 increases inositol trisphosphate receptor (IP_3R) channel opening and blocks the Ca^{2+} ATPase activity, thus emptying the ER Ca^{2+} store and thereby further activating SOCE and dye entry. Our data demonstrate the existence of complex interactions between FM4-64 and SOCE in astrocytes.

Results

Endocytosis Is Not a Major Mechanism for Astrocytic FM4-64 Uptake. Short exposure of mouse cortical astrocytes in culture to micromolar concentrations of FM4-64 (6.7 μM, 2 min) at room temperature (RT) followed by a 10-min wash showed the expected FM4-64 puncta (14, 18, 19) associated with a diffuse labeling. Rupturing the PM in zero extracellular Ca^{2+} concentration ($[Ca^{2+}]_o$) reduced the diffuse labeling without affecting the puncta (Fig. 1*A*), suggesting that background FM4-64 staining is not a result of the distribution of the dye inside small vesicles and that endocytosis and vesicle trafficking do not contribute to this background. This was confirmed by the weak co-localization found between several FM dyes and fluorescent endocytic markers (Fig. 1*B*) (20). Five-minute co-application of green FM1-43 and 3,000-MW Texas Red dextran (Tx-d) resulted in a lower correlation coefficient ($r_{12} = 0.16 \pm 0.07$, $n = 8$; see *SI Appendix*) than that found when coapplying green FM1-43 and red FM4-64 (Fig. S1*A* in *SI Appendix*; $r_{12} = 0.90 \pm 0.03$, $n = 7$). Similarly, the correlation between FM4-64 and 10,000-MW fluorescein-dextran (FL-d) was weak (Fig. S1*B* in *SI Appendix*; $r_{12} = 0.13 \pm 0.05$, $n = 18$). Both endocytic markers labeled few puncta (0.007 puncta/$\mu m^2 \pm 0.003$, $n = 9$ cells for TX-d; 0.009 puncta/$\mu m^2 \pm 0.004$, $n = 8$ for FL-d) compared with FM1-43 and FM4-64 (0.04 puncta/$\mu m^2 \pm 0.01$, $P < 0.01$ for FM1-43; 0.04 puncta/$\mu m^2 \pm 0.01$, $P < 0.01$ for FM4-64). The low density of Tx-d- and FL-d-labeled puncta was not a result of impaired endocytosis, because a 3-h incubation with either dextran produced significant vesicle labeling (0.07 puncta/$\mu m^2 \pm 0.02$, $n = 6$ cells for Tx-d; 0.06 puncta/$\mu m^2 \pm 0.03$, $n = 5$ cells for FL-d; Fig. S1*C* in *SI Appendix*). These data indicate that FM4-64 and FM1-43 uptake in astrocytes operates on time scale and labels subcellular compartments different from endocytic pathway.

Performing FM4-64 loading at 4 °C reduced the dye uptake [single-cell mean fluorescence (MF), 13.2 a.u. ± 4.0, 39% of control; 0.028 puncta/$\mu m^2 \pm 0.02$, 45% of control, $n = 13$ cells; Fig. 1*C*), suggesting that endocytosis is not a prevalent mechanism for FM4-64 entry (21). Likewise, using brefeldin A to impair vesicle trafficking (22), dynasore to inhibit the GTPase activity of dynamin (23), cytochalasin D to inhibit actin depolymerization, and jasplakinolide to stabilize actin filaments (24, 25) had no effect on astrocytic FM4-64 labeling ($P = 0.16$–0.69, $n = 7$–13; Fig. 1 *D* and

Author contributions: D.L., M.O., and N.R. designed research; D.L. and K.H. performed research; K.H. contributed new reagents/analytic tools; D.L., M.O., and N.R. analyzed data; and D.L., M.O., and N.R. wrote the paper.

The authors declare no conflict of interest.

This article is a PNAS Direct Submission.

[1]To whom correspondence may be addressed. E-mail: nicole.ropert@parisdescartes.fr or martin.oheim@parisdescartes.fr.

This article contains supporting information online at www.pnas.org/cgi/content/full/0909109106/DCSupplemental.

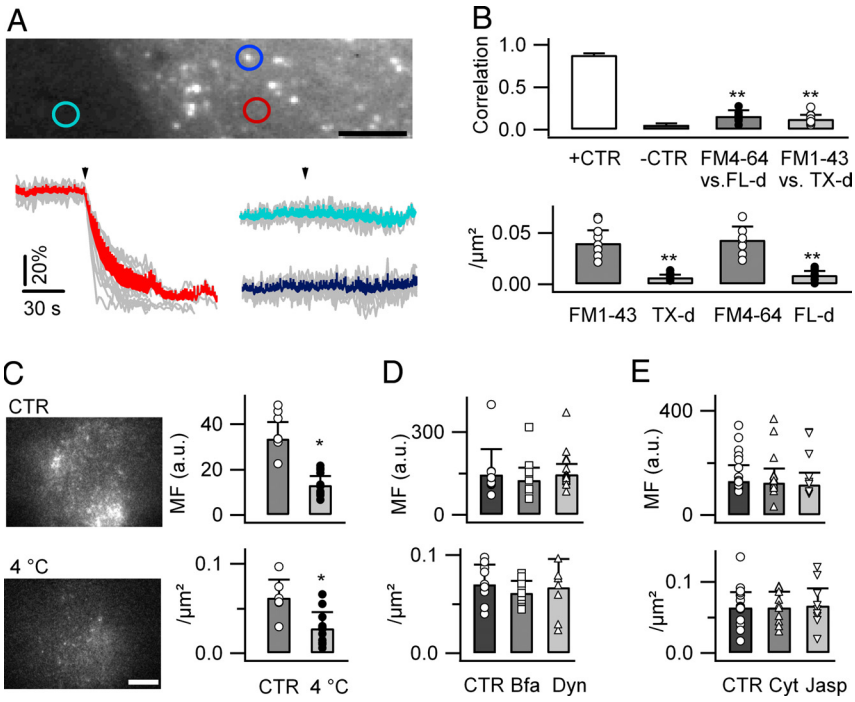

Fig. 1. Endocytosis is not a major route for rapid FM dye uptake in cultured astrocytes. (*A*) Epifluorescence image of a subregion of a cortical astrocyte loaded with FM4-64 (6.7 μM, 2 min incubation at RT, 10-min wash). (Scale bar, 5 μm.) Traces (gray, individuals; color, mean ± SD) display the evolution with time of the fluorescence intensity upon membrane rupture, measured in the extracellular (turquoise, 11 ROIs from 5 cells), cytoplasmic (red; 13 ROIs), and vesicular ROIs after local background subtraction (blue, 14 ROIs). (*B*) *Top*: Pearson correlation coefficient, calculated for subcellular ROIs between FM dyes and endocytic markers, coloaded for 5 min (Fig. S1*B* in *SI Appendix*). *Bottom*: Labeled puncta density (per μm^2). (*C*) TIRFM images of astrocytes loaded with FM4-64 (6.7 μM, 5 min) at RT (control; *CTR*) and 4 °C ($T_{chamber}$, 3.7 ± 0.4 °C, n = 25). (Scale bar: 10 μm.) (*D*) FM4-64 labeling in control and after pretreatment with brefeldin A (*Bfa*, 5 μg/mL, 30 min) or dynasore (*Dyn*, 50 μM, 30 min; P = 0.2–0.77, n = 8–15 cells per condition). (*E*) FM4-64 labeling in control and after pretreatment with cytochalasin D (*Cyt*, 5 μM, 60 min) or jasplakinolide (*Jasp*, 2 μM, 60 min; P = 0.16–0.69, n = 5–18 cells). *, $P < 0.05$; **, $P < 0.01$.

E). Finally, 24 h preincubation of astrocytes with tetanus toxin (TeNT, 2 μg/mL) to inhibit astroglial SNARE-mediated exocytosis (26) modified neither FM4-64 uptake (MF, 180.9 a.u. ± 57.8, n = 15, in TeNT vs. 178.3 a.u. ± 30.3, n = 12, in control; P = 0.51) nor puncta density (0.093 puncta/μm^2 ± 0.014 in TeNT vs. 0.087 puncta/μm^2 ± 0.03 in control; P = 0.39). These data indicate that exocytic/endocytic vesicle cycling does not contribute to FM4-64 uptake by astrocytes.

FM4-64 Permeates Through an Aqueous Pore. A diffuse non-endocytic FM1-43 fluorescence was already reported in various sensory cells (27–34). It was attributed to FM1-43 permeation through a cationic channel, the exact nature of which remained elusive.

To test if the FM dye uptake involves permeation through an aqueous pore, we compared the uptake of the small FM5-95 and the large FM3-25 with the corresponding uptake of medium-sized FM4-64 and FM1-43 dyes (10) (see *SI Appendix*). The whole-cell fluorescence can be used as a direct readout of FM5-95 and FM4-64 uptake because, when mixed with lysophosphatidylcholine (LPC) at equal concentration, both dyes have similar fluorescence intensity (Fig. S2*A* in *SI Appendix*) and excitation/emission spectra (10) (Fig. S2*B* in *SI Appendix*). The smaller FM5-95 produced a higher fluorescence of astrocytes than the medium-sized FM4-64 (MF, 534 a.u. ± 138, n = 25 cells, vs. 244 a.u. ± 139, n = 21 cells; $P <$ 0.01), and larger puncta density (0.09 puncta/μm^2 ± 0.03 vs. 0.07 puncta/μm^2 ± 0.02; $P < 0.05$; Fig. 2*A*). Similar initial fluorescence was obtained for FM3-25 and FM1-43 (Fig. S2*C* in *SI Appendix*), but the large FM3-25 could not be washed out from the PM (Fig. S2*D* in *SI Appendix*); therefore, we quenched extracellular FM3-25 with bromophenol blue (BPB) (19) to allow the quantification of FM3-25 uptake. After BPB treatment, the whole-cell fluorescence was smaller for FM3-25 than FM1-43 (MF, 32.9 a.u. ± 14.7 vs. 167.2 a.u. ± 60; n = 7; $P < 0.01$), as was the density of labeled puncta (0.01

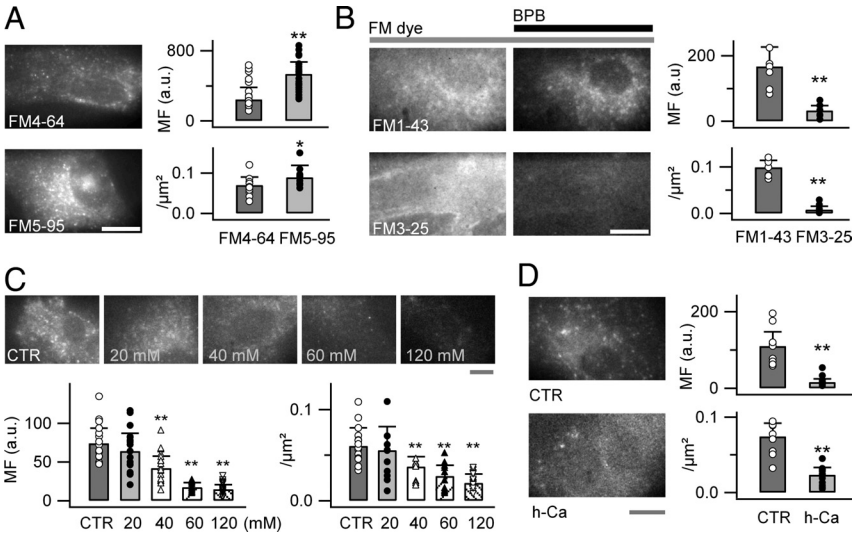

Fig. 2. FM dyes uptake in astrocytes involves a cationic channel. (*A*) Epifluorescence images of astrocytes labeled with either FM4-64 or its spectral analogue FM5-95 (6.7 μM, 5 min each). Loading is enhanced with the smaller FM5-95. (*B*) Similar labeling to FM4-64 is seen with short lipophilic tail FM1-43 (12 μM), but FM3-25 (20 μM), having a longer lipophilic tail, is virtually impermeant. Quenching extracellular FM1-43 and FM3-25 with 2 mM BPB permitted quantification of the intracellular labeling. (*C*) Incubation of the astrocytes in high $[K^+]_o$ solutions reduced FM4-64 uptake. (*D*) Incubation of the astrocytes with FM4-64 at high $[Ca^{2+}]_o$ (20 mM, *h-Ca*) diminished FM dye uptake compared with control (1.8 mM) medium [control (*CTR*); n = 7–25 cells per condition]. (Scale bars: 10 μm.)

puncta/μm^2 ± 0.01 vs. 0.1 puncta/μm^2 ± 0.02; $P < 0.01$; Fig. 2*B*). Thus, the astrocytic dye uptake during the 2- to 5-min incubation time is size-selective.

At physiological pH, permeation of the divalent FM cation (35) through an aqueous pore should be affected by the driving force across the PM. As the resting membrane potential of astrocytes is dominated by K^+ channel conductance (36) and follows the K^+ equilibrium potential, we changed the driving force on the FM dye by incubating astrocytes in FM4-64 solutions containing 5.5 to 120 mM extracellular K^+ ($[K^+]_o$), lowering extracellular Na^+ concentration accordingly. FM4-64 uptake and the density of labeled puncta correlated with $[K^+]_o$ (MF, 42.2 a.u. ± 15.4, 17.4 a.u. ± 6.1, and 14.9 a.u. ± 5.9 for 40, 60, and 120 mM $[K^+]_o$; 56.8%, 23.5%, and 20.1% of control, respectively; $P < 0.01$; n = 14–20; 0.037 puncta/μm^2 ± 0.01, 0.027 puncta/μm^2 ± 0.012, and 0.02 puncta/μm^2 ± 0.01; 62%, 43.6%, and 32.3% of control, respectively; $P < 0.01$; Fig. 2*C*). Interestingly, high $[K^+]_o$, evoked a Co^{2+}-sensitive $[Ca^{2+}]_i$ elevation (Fig. S3*A* in *SI Appendix*), but had no effect on vesicular FM4-64 labeling in astrocytes (Fig. S3*C* in *SI Appendix*). This contrasts with observations made with cultured neurons, in which the facilitation of synaptic release by high $[K^+]_o$ increased FM4-64 uptake and destaining (Fig. S3*B*–*C* in *SI Appendix*). These results strongly suggest that FM4-64 enters into astrocytes by permeating through an aqueous cationic channel rather than by endocytosis.

FM4-64 Uptake Relies on a SOCE Pathway. To identify the FM4-64-permeable channel, we first tested if FM4-64 uptake depends on the extracellular divalent cation concentration. We found that labeling the astrocytes in elevated (20 mM) $[Ca^{2+}]_o$ reduced both the whole-cell fluorescence and the density of FM4-64-labeled puncta to 15% and 32% of control in 1.8 mM Ca^{2+}, respectively ($P < 0.01$, n = 9–12 cells; Fig. 2*D*). Increasing the external Mg^{2+} concentration ($[Mg^{2+}]_o$) from 1.0 to 20 mM had no effect on the dye uptake or the density of labeled puncta (MF, 106.2 a.u. ± 35.8, 0.066 puncta/μm^2 ± 0.03, n = 11, vs. control, 128.7 a.u. ± 31.4, 0.071 puncta/μm^2 ± 0.03, n = 10; $P > 0.32$), suggesting that FM4-64 competes with Ca^{2+} for permeation through a Ca^{2+}-permeable cationic channel. A possible involvement of Ca^{2+}-permeable ligand-gated channels (TRPV, AMPA, NMDA, P2X, acetylcholine receptors), mechanotransducer channels, voltage-gated Ca^{2+} channels, inward rectifier Kir4.1 channels, and the PM Na^+-Ca^{2+} exchanger was excluded by testing the effect of specific agonists and antagonists on FM4-64 uptake (Table S1 in *SI Appendix*). We also excluded a possible role of hemichannels and volume-sensitive anion channels.

Astrocytes in culture generate spontaneous $[Ca^{2+}]_i$ elevation (Fig. S4*A* in *SI Appendix*), which is sustained by Ca^{2+} influx via the SOCE pathway (4), suggesting SOCE as a possible route for FM dye entry. Recent work identified the STIM and Orai proteins and the TRPC channels as key proteins of SOCE (4, 6–8). We found that depleting the astroglial ER Ca^{2+} stores with thapsigargin (TG, 2 μM, 30 min) increased FM4-64 uptake and the density of FM dye-labeled puncta (Fig. 3*A*; see Table S2 in *SI Appendix* for detailed quantification). To further test a possible involvement of SOCE, we used calyculin A (200 nM, 60 min), which up-regulates SOCE (37), and found that it facilitates FM dye uptake; however, it reduces the density of FM dye-labeled puncta (Fig. 3*B* and Table S2 in *SI Appendix*). Anisomycin (30 μM, 12 h), which reduces the Ca^{2+} leak from ER and the SOCE (38), reduced FM dye uptake and the puncta density (Fig. 3*C* and Table S2 in *SI Appendix*). Gd^{3+}, a nonspecific blocker of SOCE (Fig. S4 in *SI Appendix*), abolished FM4-64 uptake (Fig. 3*D* and Table S2 in *SI Appendix*). By using 3,5 bistrifluoromethyl pyrazole 2 (BTP2; 40 μM) (39) to interfere with SOCE by blocking TRPC channels, we observed a reduced FM dye uptake and puncta density (Fig. 3*E* and Table S2 in *SI Appendix*). SKF96365 (20 μM), another TRPC blocker (8), similarly decreased both parameters (Fig. 3*F* and Table S2 in *SI Appendix*). Finally,

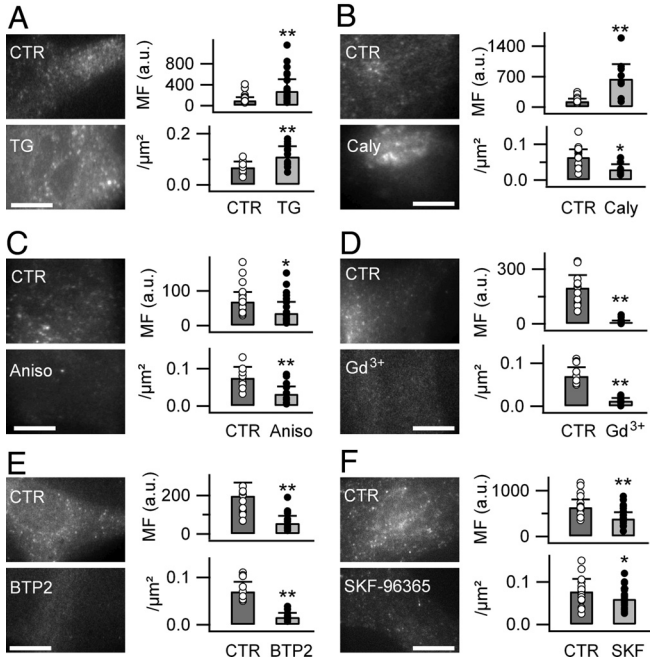

Fig. 3. FM4-64 uptake involves a SOCE pathway. FM4-64 labeling (6.7 μM, 5 min) was increased by TG treatment (2 μM, 30 min) (*A*), and calyculin A (*Caly*, 200 nM, 60 min) (*B*), and inhibited by anisomycin (*Aniso*, 30 μM, 12 h) (*C*), Gd^{3+} (100 μM, 10 min) (*E*), BTP2 (40 μM, 10 min) (*D*), and SKF96365 (20 μM, 10 min) (*F*).

2-aminoethoxy diphenylborate (2-APB) applied at a concentration that blocks Orai1 (100 μM, 10 min) (40) increased the FM4-64 uptake and the puncta density (Table S1 in *SI Appendix*). These results suggest that the permeant FM4-64 enters astrocytes via SOCE channels and that a TRPC-like rather than a Orai1 channel forms the pore for the dye entry.

FM4-64 Activates SOCE by Interacting with the PM Lipid Bilayer. The insertion of lipids in the PM alters the lipid rafts (41), the activity of ionic channels (42), SOCE (4), as well as TRPC/Orai interaction (6). Amphiphilic FM dyes alter the lipid arrangement (35) and the PM mechanical properties (43), suggesting that their insertion in the PM could affect the activity of the store-operated channels.

This possibility was tested by studying first the effect on FM4-64 uptake of the spider *Grammostola spatulata* mechanotoxin *peptide 4* (GsMTx-4), an inhibitor of stretch-activated mechanosensitive channels and SOCE (44) that modifies the PM lipid/channel interaction. We found that 5 μM GsMTx-4 reduced FM4-64 uptake and puncta density (Fig. 4*A* and Table S2 in *SI Appendix*). Likewise, LPC (5 μM), which facilitates SOCE (4), enhanced the FM4-64 uptake and puncta density (Fig. 4*B* and Table S2 in *SI Appendix*). Arachidonic acid (10 μM), a lipid with no effect on SOCE (4), did not alter FM4-64 uptake (Fig. 4*B*). Finally, methyl-β-cyclodextrin (MβCD), which disrupts lipid rafts by sequestering cholesterol, reduced astrocytic FM4-64 uptake and puncta density (Fig. 4*C* and Table S2 in *SI Appendix*). Our results show that FM4-64 insertion in the outer leaflet of the PM, and the subsequent change of the membrane mechanical properties that can change the SOCE, might interfere with FM4-64 uptake.

To more directly test the lipid-mediated effect of styryl dyes on SOCE, we studied the effect of the non-permeant (Fig. 2*B*) green FM3-25 on $[Ca^{2+}]_i$ using a red-fluorescent Ca^{2+} indicator Xrhod-1, acetoxymethyl ester (AM). We used total internal reflection fluorescence (TIRF) microscopy to monitor near-membrane $[Ca^{2+}]_i$ (Fig. 4*D*). FM3-25 was applied with a small (250 μm ID) silica pipette (Fig. S5*A1* in *SI Appendix*) positioned close to the astrocyte. We verified that the local application of control buffer on intact

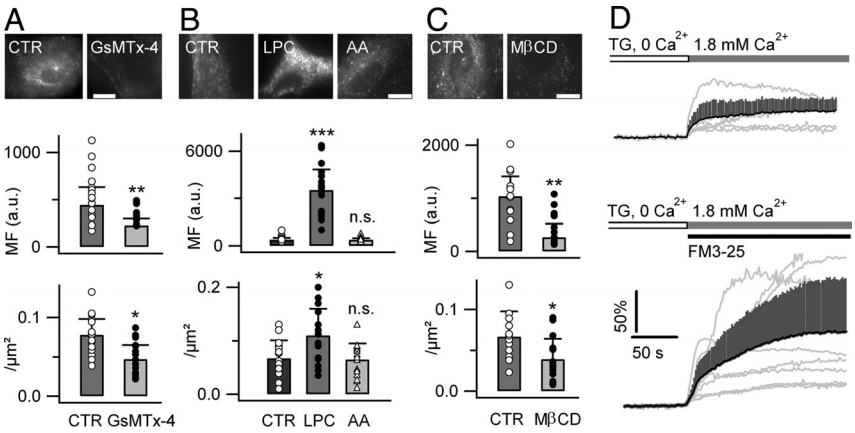

Fig. 4. FM dye insertion in the PM outer lipid leaflet activates a SOCE. (*A*) Preincubating astrocytes with GsMTx-4 (5 μM, 10 min) reduced the FM4-64 uptake (6.7 μM, 5 min). (*B*) Treating astrocytes with LPC (5 μM, 10 min) increased the FM4-64 uptake. Arachidonic acid (*AA*, 10 μM, 10 min) had no effect. (*C*) Treating astrocytes with MβCD (10 mM, 1 h) diminished FM4-64 labeling. (*D*) The local application of green impermeant FM3-25 facilitated SOCE. The ER store was depleted by treating cells with TG (1 μM, 10 min) in Ca^{2+}-free buffer. The $[Ca^{2+}]_i$ was monitored with the red Ca^{2+} indicator Xrhod-1 (n = 7–16 cells per condition). (Scale bars: 10 μm.)

astrocytes did not trigger an appreciable $[Ca^{2+}]$ change [dF/F_0, 0.01 ± 0.03, n = 7 cells, vs. control, 0.01 ± 0.02, n = 9 cells (P = 0.93), measured in static solution over the same period]. When astrocytes were pretreated with TG (1 μM, 10 min) in a Ca^{2+}-free buffer to deplete the ER store, locally applying 1.8 mM $[Ca^{2+}]_o$ induced a SOCE-mediated $[Ca^{2+}]_i$ elevation (dF/F_0, 0.37 ± 0.2, n = 7 cells) that only slowly returns to baseline, as a result of the partial mitochondrial localization of Xrhod-1 (*SI Methods* in *SI Appendix*). Simultaneously applying 10 μM FM3-25 and 1.8 mM $[Ca^{2+}]_o$ induced a larger $[Ca^{2+}]_i$ elevation (dF/F_0, 0.9 ± 0.6, n = 11 cells; $P < 0.05$), as expected if FM3-25 recruits additional SOCE channels. These results indicate that the FM3-25 insertion into the PM of astrocytes facilitates the SOCE channel gating .

Effect of Permeant FM4-64 on the Ca^{2+} Signaling in Astrocytes. FM4-64 competes with Ca^{2+} and therefore should act as a permeant store-operated channel blocker, like FM1-43 for the mechanotransducer channels (28). Using the same protocol as in Fig. 4*D*, we studied the effect of 6.7 μM FM4-64 on the $[Ca^{2+}]_i$ measured with Oregon green BAPTA–1 [2,2′-(ethylenedioxy)dianiline-N,N,N′,N′-tetraacetic acid; OGB-1; Fig. 5*A*]. Unlike the nonpermeant FM3-25, FM4-64 reduced SOCE (dF/F_0, 0.22 ± 0.2, n = 9, with FM4-64 vs. 0.97 ± 0.12, n = 6, in control; $P < 0.01$). Thus, in addition to facilitating the gating of the SOCE channels, the permeant FM4-64 behaves as a channel blocker of the SOCE in cortical astrocytes.

We then studied the effect of the permeant FM4-64 on the astroglial Ca^{2+} signaling in standard 1.8 mM $[Ca^{2+}]_o$ to directly correlate the dye insertion in the PM and its cellular uptake with astroglial Ca^{2+} signaling in nondepleted Ca^{2+} store condition. We used a double-pulse protocol in which control and FM4-64-containing solutions were sequentially applied to OGB-1-loaded cells through the local perfusion pipette as used for Fig. 4*D* (see *SI Text* and Fig. S5*A* in *SI Appendix*). When applying control solution, no $[Ca^{2+}]_i$ changes were observed (Fig. S6 in *SI Appendix*). Upon addition of FM4-64, the insertion of the dye in the PM was detected as a rapid red fluorescence increase, followed by a slower increase as expected from dye uptake. Even the small leak of FM4-64 observed upon actuating the application of control buffer triggered a $[Ca^{2+}]_i$ increase (dF/F_0, 0.13 ± 0.05, n = 5 cells). The FM4-64 application itself evoked a robust $[Ca^{2+}]_i$ increase (peak dF/F_0, 0.43 ± 0.1, n = 10 cells) that followed the FM dye red fluorescence by 5.7 s ± 2.9 (n = 6) measured as the half-maximal delay (Fig. 5*B Inset*). This $[Ca^{2+}]_i$ elevation in astrocytes contrasts with the absence of response by neurons $[Ca^{2+}]_i$ following the same FM4-64 application (Fig. S8 in *SI Appendix*). Washing FM4-64 leading to an early fast reduction of the red fluorescence as a result of the rapid departitioning of the dye from the PM was followed by a slower

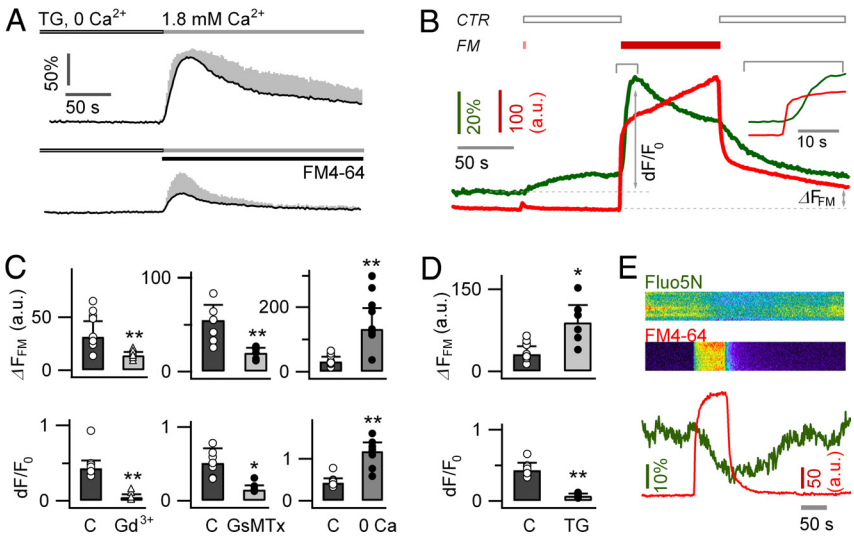

Fig. 5. Permeant FM dyes modifies Ca^{2+} signaling in cultured astrocytes. (*A*) After depletion of ER Ca^{2+} store with TG in 0 mM Ca^{2+}, an SOCE was induced by local application of control (*CTR*) solution (1.8 mM Ca^{2+}, *Upper*) or by CTR solution containing 6.7 μM FM4-64 (*Lower*). Monitoring $[Ca^{2+}]_i$ with the green Ca^{2+} indicator OGB-1, we show that FM4-64 reduces the SOCE (mean ± SD, black and gray traces). (*B*) We locally applied control solution (1.8 mM Ca^{2+}; *CTR*) first, followed by the application of FM4-64-containing solution (6.7 μM FM4-64 and 1.8 mM Ca^{2+}; *FM*), before returning to the control. FM4-64 evokes a $[Ca^{2+}]_i$ elevation (green trace) that follows the FM dye insertion inside the outer PM lipid leaflet (red trace), measured with TIRFM. *Inset*: Same traces magnified to show the onset of the response to FM4-64. (*C*) Gd^{3+} (100 μM) and GsMTx-4 (2.5 μM) both reduced FM4-64 uptake (ΔF_{FM} measured at the end of the 2 min FM4-64 wash, *B*) and the FM-triggered $[Ca^{2+}]_i$ transient (dF/F_0 measured at the peak of the Ca^{2+} response, *B*). Removing extracellular Ca^{2+} (0 Ca^{2+}, 5 mM EGTA) facilitated both the FM4-64 uptake and the Ca^{2+} response. (*D*) Pretreatment of astrocytes with TG (2 μM, 20 min) enhanced FM4-64 uptake and suppressed the FM dye-induced mobilization of intracellular Ca^{2+} store. (*E*) In astrocytes transfected with an ER-targeted esterase, local application of FM4-64 (6.7 μM) induced a reduction of the ER Ca^{2+} concentration ($[Ca^{2+}]_{ER}$) monitored with the low-affinity Ca^{2+} indicator fluo5N-AM. *Top*: Dual-color Fluo5N and FM4-64 TIRFM kymographs. *Bottom*: FM4-64 insertion into the PM (red trace) was associated with a reduction of $[Ca^{2+}]_{ER}$ (green trace; n = 5–10 cells per condition).

reduction, probably as a result of the permeation of the dye through an SOCE channel. A residual red fluorescence (ΔF_{FM}) was attributed to dye uptake. The FM4-64-induced $[Ca^{2+}]_i$ elevation was concentration-dependent and saturated at relatively low concentration (approximately 1 μM; Fig. S7*A* in *SI Appendix*).

Using the same protocol (Fig. 5*C*), we showed that, in astrocytes, the FM4-64-induced $[Ca^{2+}]_i$ elevation was suppressed by GsMTx-4 (dF/F_0, 0.15 ± 0.06, $n = 5$, in GsMTx-4 vs. 0.51 ± 0.2, $n = 7$, in control; $P < 0.01$) and Gd^{3+} (dF/F_0, 0.05 ± 0.04, $n = 5$, in Gd^{3+} vs. 0.4 ± 0.1, $n = 7$, in control; $P < 0.01$). Dye uptake was also reduced by GsMTx-4 (ΔF_{FM}, 19.6 a.u. ± 5.4 in GsMTx-4 vs. 54.9 a.u. ± 16.3 in control; $P < 0.01$) and by Gd^{3+} (ΔF_{FM}, 14.03 a.u. ± 3.2 in Gd^{3+} vs. 31.3 a.u. ± 14.9 in control; $P < 0.01$). In 0 mM $[Ca^{2+}]_o$, the local application of FM4-64 induced a larger $[Ca^{2+}]_i$ increase (279% of control; dF/F_0, 1.2 ± 0.2; $n = 10$; $P < 0.01$) and a larger FM4-64 uptake to 423% of control (ΔF_{FM}, 132.5 a.u. ± 64.3; $P < 0.01$; Fig. 5*C*). This is consistent with our previous conclusion (see Fig. 2*D*) that FM dye and Ca^{2+} compete for the same channel and that Ca^{2+} removal facilitates FM entry (and vice versa). Depleting the ER Ca^{2+} store with TG (2 μM, 30 min) enhanced the FM4-64-triggered FM dye uptake (ΔF_{FM}, 89.5 a.u. ± 31.8 in TG vs. 31.3 a.u. ± 14.9 in control; $P < 0.01$) and reduced the evoked Ca^{2+} response (dF/F_0, 0.07 ± 0.03, $n = 9$, in TG vs. 0.43 ± 0.10, $n = 10$ cells, in control; $P < 0.01$; Fig. 5*D*). These data suggest FM dye entry as a prerequisite for the trigger of Ca^{2+} response and the internal store as a major Ca^{2+} source for the response.

To directly monitor the possible release of Ca^{2+} from the ER by FM dyes, we measured the $[Ca^{2+}]_{ER}$ by transfecting the astrocytes with a recombinant ER-targeted carboxyl esterase (CES-2) to facilitate the accumulation of the low-affinity Ca^{2+} indicator Fluo-5N AM (K_d, approximately 90 μM) to the ER (45). The local application of 6.7 μM FM4-64 on the transfected astrocytes evoked a rapid reduction (12 ± 4% in 60 s) of Fluo-5N fluorescence (dF/F_0, −0.21 ± 0.1, $n = 5$; Fig. 5*E*), confirming that FM4-64 facilitates the Ca^{2+} release from the ER. Finally, we tested the effect of 10 mM caffeine, a blocker of IP_3R (46), which abolished most FM dye-evoked Ca^{2+} signal (dF/F_0, 0.08 ± 0.03, 35% of its control value, $n = 5$; $P < 0.01$; Fig. S9*A* in *SI Appendix*). Ryanodine (1 μM, 1 h) had no effect on the FM4-64-evoked Ca^{2+} response ($n = 6$–7; $P = 0.62$; Fig. S9*B* in *SI Appendix*). Together, these results indicate that FM dye-evoked Ca^{2+} responses are caused by Ca^{2+} release through IP_3R channels from a TG-sensitive ER store.

Discussion

We demonstrate that astroglial FM dye uptake does not involve endocytosis but an aqueous pore, and that it profoundly affects Ca^{2+} homeostasis of astrocytes. We show that both dye uptake and the associated $[Ca^{2+}]_i$ elevation involve a SOCE pathway, suggesting that the permeant FM dyes enter astrocytes via a SOCE channel, i.e., a STIM/Orai/TRPC complex. We also show that FM dyes modify astroglial Ca^{2+} signaling by acting at several levels (Fig. S10 in *SI Appendix*): (*i*) the FM dye insertion into the outer leaflet of the PM facilitates the gating of the SOCE; (*ii*) the FM dyes compete with Ca^{2+} for permeating across the SOCE channel; (*iii*) intracellular FM dye mobilizes Ca^{2+} from the ER store, conveying a positive feedback signal to activate SOCE and sustain dye uptake into astrocytes.

FM Dye Within Astrocytes Contributes to a Diffuse Background in the Brain Slices. Early studies introducing FM dyes as fluorescent probes to investigate secretory vesicle cycling in nerve terminals reported a stimulation-insensitive FM dye labeling in Schwann cells (9), but this observation received little attention. In brain slice, FM dye labeling produces a strong background that can be quenched by sulforhodamine 101 (47, 48), a selective marker of astrocytes (49). Our results suggest that the FM1-43 background seen in the slice is due to the astroglial activity-independent FM dye uptake which is quenched by sulforhodamine 101. It suggests that the FM dye distribution within astrocyte in the slice preparation shares similarities with the distribution we found here in astrocytes in culture. However, whether all our findings apply to the astrocytes in situ will need further investigation.

FM Dye Enters Through a TRP-Like Channel. Our study does not support endocytosis as a major route for the rapid FM dye entry into cortical astrocytes (Fig. 1). Rather, the dependence of the dye uptake on its molecular size and on the electrical driving force across the PM (Fig. 2) indicate that the FM dyes enter through a cationic aqueous pore. Earlier reports have already suggested that FM dyes permeate through cationic channels (28, 30, 31). The temperature sensitivity of the dye uptake (Fig. 1*C*) is compatible with the thermosensitivity of ion channels in general (50) and of TRP channels (51). The dye uptake is sensitive to TG, calyculin A, anisomycin, Gd^{3+}, and SKF96365 (Fig. 3), which interfere with SOCE; and to GsMTx-4 and LPC, which affect the interaction between the PM lipid bilayer and the SOCE (Fig. 4). The implication of SOCE is also evidenced by showing that the FM dye insertion into the PM interferes directly with Ca^{2+} permeation through a SOCE channel (Fig. 4*D*) and depletes the ER Ca^{2+} stores (Fig. 5*D*). Finally, our findings that the FM dye uptake is sensitive to BTP2, a blocker of TRPC channels (8), and to 2-APB, a blocker of the Orai proteins (40), indicate that the FM dyes permeate through a STIM1/Orai/TRPC complex. The implication of TRP channels is compatible with their expression by astrocytes (2, 3, 52, 53). The sensitivity of the FM dye uptake to Gd^{3+}, BTP2, GsMTx-4, MβCD, and LPC is compatible with the involvement of a TRPC-like channel. The effect of 2-APB that inhibits several TRPC channels at 5 to 20 μM, activates TRPV1–3 channels, and has no effect on TRPV4 (54), suggests that the astroglial FM dye uptake might involve also TRPV1–3 channels. Our earlier report that the mechanical stimulation of astrocytes triggered astroglial $[Ca^{2+}]_i$ elevation and a loss of a diffuse intracellular FM dye signal (19) is also compatible with the permeation of the FM dye through mechanosensitive TRP-like channels (55). In conclusion, the permeant FM dyes appear to enter the astrocytes via a TRPC/TRPV-like channel, but the exact stoichiometry of the channel is still uncertain and will require more specific tools such as siRNAs.

Permeant FM Dyes Facilitate ER Store Depletion and FM Dye Entry. Our data show that, when in the cytosol, the permeant FM dyes facilitate ER store depletion (Fig. 5*D*), either by enhancing Ca^{2+} efflux through the IP_3R channel as indicated by the effect of caffeine (Fig. S8*A* in *SI Appendix*) or by reducing the sarcoplasmic/endoplasmic reticulum Ca^{2+} ATPase activity (56). Such a depletion of the ER Ca^{2+} store should act as a positive feedback loop to enhance the FM dye uptake through the STIM/Orai/TRPC complex and overcome the partial block of the cationic channel by the permeant FM dyes. Previous observations indicate that FM dye accumulate inside lysosomes (18, 19). Our finding of a correlation between the whole-cell fluorescence and the puncta density suggests that the permeant FM dyes traffic from the cytosol to the lysosomal lumen but the mechanism is unknown.

The absence of diffuse neuronal FM dye labeling is surprising given that SOCE, Orai1, STIM1, and TRPC1 are expressed by neurons (57). One reason might be a different channel density, because in neurons Ca^{2+} influx is mostly caused by voltage-gated Ca^{2+} channels, whereas the astroglial Ca^{2+} signaling is dominated by SOCE and relies on the near-membrane ER to rapidly replenish the ER stores (2). The repertoire of TRP channels expressed by astrocytes might also be uniquely favorable to FM dye permeation.

Materials and Methods

For detailed description of experimental procedures, see *SI Text* in *SI Appendix*.

Cell Culture and Dye Loading. We used low-density cortical astrocytes from newborn mice maintained in culture as previously described (19). Control exper-

iments were done on cortical neurons from embryonic mice. Dye loading and recordings were made at RT in solution containing (in mM): 140 NaCl, 5.5 KCl, 1.8 $CaCl_2$, 1 $MgCl_2$, 20 glucose, 10 Hepes (pH 7.3, NaOH). Astrocytes were labeled with 6.7 μM FM1-43, FM4-64, or FM5–95 in static bath for 2 to 5 min, followed by a 10-min wash. During recording, cells were constantly perfused at 0.5 to 1 mL/min with standard solution.

Ca^{2+} Imaging and Co-Localization Studies. A custom-built inverted microscope was used for bright-field, polychromatic epi- and through-the-objective TIRF microscopy. 476-, 488- or 568-nm lines from the beam of an Ar^+/Kr^+ multiline laser were used for TIRF microscopy. The near-membrane $[Ca^{2+}]_i$ transients are shown after photobleaching correction as dF/F_0 with TIRFM using nonratiometric Ca^{2+} indicators, OGB-1-AM together with FM4-64/FM5-95 or Xrhod-1-AM together with FM3-25. The ER Ca^{2+} change was monitored using the low-affinity Ca^{2+} indicator Fluo-5N AM selectively targeted to the ER lumen by transfecting a ER-targeted recombinant CES-2 (provided by Robert Blum, Münich, Germany) 24 to 36 h before imaging. All combinations of excitation wavelengths, dichroics, and filters used are listed in Table S3 in *SI Appendix*. Colocalization was assessed by calculating the Pearson correlation coefficient r_{12}.

The density of fluorescent organelles was measured after high-pass filtering, thresholding, and watershed segmentation. Particle number was normalized with total area, estimated for epifluorescence images, from the threshold contour of the cell and, for TIRF images, from the size of the region of interest. MF was measured within their contour, after subtraction of the average mean autofluorescence measured in the corresponding color channel from nonlabeled cells of the same preparation. For each pharmacological condition, control and treated measurements of MF and particle density were performed on paired cells from the same preparation.

ACKNOWLEDGMENTS. We thank Thibault Collin (Paris, France) and Reinaldo DiPolo (Caracas, Venezuela) for helpful discussions, Robert Blum (Munich, Germany) for the gift of the CES-2 plasmid, and Hans-Jürgen Apell (Konstanz, Germany) for sharing unpublished observations on interactions of styryl dyes with sarcoplasmic Ca^{2+}-ATPase. D.L. received a postdoctoral fellowship from the Agence Nationale de la Recherche (ANR). This work was funded by ANR Neuroscience, Neurologie, et Neuropsychiatrie Grant APV05116KSA, ANR PNANO Grant RPV06020KKA, and European Union 6PCRD (Autoscreen, 0307897).

1. Beck A, Nieden RZ, Schneider HP, Deitmer JW (2004) Calcium release from intracellular stores in rodent astrocytes and neurons in situ. *Cell Cal* 35:47–58.
2. Golovina VA (2005) Visualization of localized store-operated calcium entry in mouse astrocytes. Close proximity to the endoplasmic reticulum. *J Physiol* 564:737–749.
3. Malarkey E, Ni Y, Parpura V (2008) Ca^{2+} entry through TRPC1 channels contributes to intracellular Ca^{2+} dynamics and consequent glutamate release from rat astrocytes. *Glia* 56:821–835.
4. Singaravelu K, Lohr C, Deitmer JW (2006) Regulation of store-operated calcium entry by calcium-independent phospholipase A_2 in rat cerebellar astrocytes. *J Neurosci* 26:9579–9592.
5. Barres BA (2008) The mystery and magic of glia: a perspective on their roles in health and disease. *Neuron* 60:430–440.
6. Liao Y, et al. (2009) A role for Orai in TRPC-mediated Ca^{2+} entry suggests that a TRPC:Orai complex may mediate store and receptor operated Ca^{2+} entry. *Proc Natl Acad Sci USA* 106:3202–3206.
7. Frischauf I, et al. (2008) The STIM/Orai coupling machinery. *Channels* 2:261–268.
8. Birnbaumer L (2009) The TRPC class of ion channels: a critical review of their roles in slow, sustained increases in intracellular Ca^{2+} concentrations. *Annu Rev Pharmacol Toxicol* 49:395–426.
9. Betz WJ, Mao F, Bewick G (1992) Activity-dependent fluorescent staining and destaining of living vertebrate motor nerve terminals. *J Neurosci* 12:363–375.
10. Betz WJ, Mao F, Smith CB (1996) Imaging exocytosis and endocytosis. *Curr Opin Neurobiol* 6:365–371.
11. Rizzoli SO, Betz WJ (2005) Synaptic vesicle pools. *Nat Rev Neurosci* 6:57–69.
12. Cali C, Marchaland J, Regazzi R, Bezzi P (2008) SDF 1-alpha (CXCL12) triggers glutamate exocytosis from astrocytes on a millisecond time scale: Imaging analysis at the single-vesicle level with TIRF microscopy. *J Neuroimmunol* 198:82–91.
13. Chen X, et al. (2005) ''Kiss-and-Run'' glutamate secretion in cultured and freshly isolated rat hippocampal astrocytes. *J Neurosci* 25:9236–9243.
14. Jiang M, Chen G (2009) Ca^{2+} regulation of dynamin-independent endocytosis in cortical astrocytes. *J Neurosci* 29:8063–8074.
15. Krzan M, et al. (2003) Calcium-dependent exocytosis of atrial natriuretic peptide from astrocytes. *J Neurosci* 23:1580–1583.
16. Marchaland J, et al. (2008) Fast subplasma membrane Ca^{2+} transients control exo-endocytosis of synaptic-like microvesicles in astrocytes. *J Neurosci* 28:9122–9132.
17. Xu J, et al. (2007) Glutamate-induced exocytosis of glutamate from astrocytes. *J Biol Chem* 282:24185–24197.
18. Zhang Z, et al. (2007) Regulated ATP release from astrocytes through lysosome exocytosis. *Nat Cell Biol* 9:945–953.
19. Li D, Ropert N, Koulakoff A, Giaume C, Oheim M (2008) Lysosomes are the major vesicular compartment undergoing Ca^{2+}-regulated exocytosis from cortical astrocytes. *J Neurosci* 28:7648–7658.
20. Martinez I, et al. (2000) Synaptotagmin VII regulates Ca^{2+}-dependent exocytosis of lysosomes in fibroblasts. *J Cell Biol* 148:1141–1150.
21. Schaeffer S, Raviola E (1978) Membrane recycling in the cone cell endings of the turtle retina. *J Cell Biol* 79:802–825.
22. Klausner R, Donaldson J, Lippincott-Schwartz J (1992) Brefeldin A: insights into the control of membrane traffic and organelle structure. *J Cell Biol* 116:1071–1080.
23. Macia E, et al. (2006) Dynasore, a cell-permeable inhibitor of dynamin. *Dev Cell* 10:839–850.
24. Qualmann B, Kessels MM, Kelly RB (2000) Molecular links between endocytosis and the actin cytoskeleton. *J Cell Biol* 150:F111–F116.
25. Yarar D, Waterman-Storer CM, Schmid SL (2005) A dynamic actin cytoskeleton functions at multiple stages of clathrin-mediated endocytosis. *Mol Biol Cell* 16:964–975.
26. Bezzi P, et al. (1998) Prostaglandins stimulate calcium-dependent glutamate release in astrocytes. *Nature* 391:281–285.
27. Crumling MA, et al. (2009) P2X antagonists inhibit styryl dye entry into hair cells. *Neuroscience* 161:1144–1153.
28. Gale JE, Marcotti W, Kennedy HJ, Kros CJ, Richardson GP (2001) FM1-43 dye behaves as a permeant blocker of the hair-cell mechanotransducer channel. *J Neurosci* 21:7013–7025.
29. Mazzone SB (2004) Sensory regulation of the cough reflex. *Pulm Pharmacol Ther* 17:361–368.
30. Meyers JR, et al. (2003) Lighting up the senses: FM1-43 loading of sensory cells through nonselective ion channels. *J Neurosci* 23:4054–4065.
31. Nishikawa S, Sasaki F (1996) Internalization of styryl dye FM1-43 in the hair cells of lateral line organs in Xenopus larvae. *J Histochem Cytochem* 44:733–741.
32. Nishikawa S (2006) Systemic labeling and visualization of dental sensory nerves by the novel fluorescent marker AM1-43. *Anat Sci Int* 81:181–186.
33. Rouze NC, Schwartz EA (1998) Continuous and transient vesicle cycling at a ribbon synapse. *J Neurosci* 18:8614–8624.
34. Yang X, Liu R (2006) Intraganglionic laminar endings act as mechanoreceptors of vagal afferent nerve in guinea pig esophagus. *Sheng Li Xue Bao* 58:171–176.
35. Schote U, Seelig J (1998) Interaction of the neuronal marker dye FM1-43 with lipid membranes: Thermodynamics and lipid ordering. *Biochim Biophys Acta* 1415:135–146.
36. Olsen M, Sontheimer H (2008) Functional implications for Kir4.1 channels in glial biology: from K^+ buffering to cell differentiation. *J Neurochem* 107:589–601.
37. Albert AP, Large WA (2002) Activation of store-operated channels by noradrenaline via protein kinase C in rabbit portal vein myocytes. *J Physiol* 544:113–125.
38. Flourakis M, et al. (2006) Passive calcium leak via translocon is a first step for iPLA2-pathway regulated store operated channels activation. *FASEB J* 20:1215–1217.
39. Zitt C, et al. (2004) Potent inhibition of Ca^{2+}-release-activated Ca^{2+} channels and T-lymphocyte activation by the pyrazole derivative BTP2. *J Biol Chem* 279:12427–12437.
40. Feske S, et al. (2006) A mutation in Orai1 causes immune deficiency by abrogating CRAC channel function. *Nature* 441:179–185.
41. Piomelli D, Astarita G, Rapaka R (2007) A neuroscientist's guide to lipidomics. *Nat Rev Neurosci* 8:743–754.
42. Lundbaek JA (2008) Lipid bilayer-mediated regulation of ion channel function by amphiphilic drugs. *J Gen Physiol* 131:421–429.
43. Zhu Y, Stevens CF (2008) Probing synaptic vesicle fusion by altering mechanical properties of the neuronal surface membrane. *Proc Natl Acad Sci USA* 105:18018–18022.
44. Suchyna TM, Sachs F (2007) Mechanosensitive channel properties and membrane mechanics in mouse dystrophic myotubes. *J Physiol* 581:369–387.
45. Rehberg M, Lepier A, Solchenberger B, Osten P, Blum R (2008) A new non-disruptive strategy to target calcium indicator dyes to the endoplasmic reticulum. *Cell Cal* 44:386–399.
46. Ehrlich BE, Kaftan E, Bezprozvannaya S, Bezprozvanny I (1994) The pharmacology of intracellular Ca^{2+}-release channels. *Trends Pharmacol Sci* 15:145–149.
47. Pyle JL, Kavalali ET, Choi S, Tsien RW (1999) Visualization of synaptic activity in hippocampal slices with FM1-43 enabled by fluorescence quenching. *Neuron* 24:803–808.
48. Stanton PK, Heinemann U, Muller W (2001) FM1-43 imaging reveals cGMP-Dependent long-term depression of presynaptic transmitter release. *J Neurosci* 21:RC167.
49. Nimmerjahn A, Kirchhoff F, Kerr JN, Helmchen F (2004) Sulforhodamine 101 as a specific marker of astroglia in the neocortex in vivo. *Nat Methods* 1:31–37.
50. Hille B (2001) Ion Channels of Excitable Membranes (Sinauer Associates, Sunderland, MA), 3rd Ed.
51. Talavera K, Voets T, Nilius B (2008) Mechanisms of thermosensation in TRP channels. *Sensing with Ion Channels*, ed Martinac B (Springer, Heidelberg), pp 101–120.
52. Benfenati V, et al. (2007) Expression and functional characterization of transient receptor potential vanilloid-related channel 4 (TRPV4) in rat cortical astrocytes. *Neuroscience* 148:876–892.
53. Kauer JA, Gibson HE (2009) Hot flash: TRPV channels in the brain. *Trends Neurosci* 32:215–224.
54. Hu HZ, et al. (2004) 2-Aminoethoxydiphenyl Borate is a common activator of TRPV1, TRPV2, and TRPV3. *J Biol Chem* 279:35741–35748.
55. Christensen AP, Corey DP (2007) TRP channels in mechanosensation: direct or indirect activation? *Nat Rev Neurosci* 8:510–521.
56. Butscher C, Roudna M, Apell HJ (1999) Electrogenic partial reactions of the SR-Ca-ATPase investigated by a fluorescence method. *J Membr Biol* 168:169–181.
57. Klejman ME, et al. (2009) Expression of STIM1 in brain and puncta-like co-localization of STIM1 and ORAI1 upon depletion of Ca2+ store in neurons. *Neurochem Int* 54:49–55.